High-Resolution Large Scale Ocean Modeling

Eric P. Chassignet and Xiaobiao Xu

Center for Ocean-Atmospheric Prediction Studies (COAPS)

Florida State University

Corresponding author: echassignet@fsu.edu

Abstract

Eddying global ocean models are now routinely used for ocean prediction and the value-added of a better representation of the observed ocean variability and western boundary currents at that resolution is currently being evaluated in climate models. In this overview article, we first provide a brief summary of the impact on ocean model biases of resolving eddies in several global ocean-sea ice numerical simulations. We then show in a series of North and Equatorial Atlantic configurations that an increase of the horizontal resolution from eddy-resolving to submesoscale-enabled together with the inclusion of high-resolution bathymetry and tides significantly improve the models' ability to represent the observed ocean variability and western boundary currents. However, the computational cost of these simulations is extremely large and, for these simulations to become routine, close collaborations with computer scientists are essential to ensure that numerical codes can take full advantage of the latest computing architecture.

1. Introduction

In the late 90s, Paiva et al. (1999) and Smith et al. (2000) showed that a minimum resolution of 1/10° was required for a reasonable representation of mid-latitudes western boundary currents and associated eddies. It is, however, generally recognized that 1/10° is not sufficient to resolve the Rossby radius of deformation everywhere (Hallberg, 2013) and, consequently, does not allow for a proper representation of baroclinic instability and associated eddies throughout the domain. This class of models, which used to be referred to as eddy-resolving, is now referred to as eddying models. Furthermore, a model's effective resolution, which depends on its inherent numerical dissipation, is on the order of $6\Delta x$ (Soufflet et al., 2016). In order to be truly eddy-resolving everywhere, the horizontal resolution of an ocean model therefore needs to be on the order of a few kilometers. When the grid spacing becomes of O(1) km, submesoscale motions of O(10) km are resolved at mid-latitudes. However, because of the computing cost at that resolution, only a few modeling studies have investigated the impact of these resolved submesoscale features on the large scale oceanic circulation (Hurlburt and Hogan, 2000; Levy et al., 2010; Chassignet and Xu, 2017). Submesoscale physics plays a significant role in the vertical fluxes of mass, buoyancy, and tracers (Thomas et al., 2008; Capet et al., 2008; Fox-Kemper et al., 2008; Klein et al., 2011; Roullet et al., 2012; Capet et al., 2016) and Chassignet and Xu (2017) argues that the next threshold for a significant improvement in western boundary currents representation (i.e., the Gulf Stream in their paper) is an increase in the horizontal resolution from an eddying 1/10° to a submesoscale-enabled 1/50° grid spacing. They showed that, as the resolution is increased to 1/50° (~ 1.5 km at mid-latitudes) from 1/12°, the representation of Gulf Stream penetration and associated recirculating gyres in their model shifts from unrealistic to realistic and the penetration of EKE into the deep ocean is drastically different and more closely resembles observations. In this overview paper on high-resolution large scale ocean modeling, after some background statements (section 2), we first discuss the impact of eddies in global ocean-sea ice numerical simulations by summarizing the comparison of coarse (~1º) and eddying (~0.1º) experiments performed by Chassignet et al. (2020a), all forced with the same atmospheric dataset (section 3). We then describe in section 4 the impact of further increasing the horizontal resolution and resolving submesoscale features in a series of North Atlantic regional configurations performed with the HYbrid Coordinate Ocean Model (Bleck, 2002; Chassignet et al., 2003). We end in section 5 with an outlook to future developments of high-resolution ocean modeling.

2. Background

As stated by Le Sommer et al. (2018), there is a wide range of uses and applications of ocean circulation models. Ocean circulation models are first and foremost used in idealized and realistic configurations to test hypotheses for any mechanisms underlying oceanic observations. When coupled to other components of the earth system (i.e., atmosphere, land, ice, etc.), they can be used to look at phenomena on seasonal to decadal time scales or to determine scenarios for the earth's climate arising from changes in anthropogenic forcing. However, numerical models are only an approximation of reality since current computational power is not sufficient to model the ocean everywhere down to the turbulent scale, i.e. the Kolmogorov length scale, which is on O(1) cm (Smyth et al., 2001). Simulations that resolve turbulence are called Direct Numerical Simulations (DNS) and can only be integrated on scales of the order of tens of meters (Yeung et al., 2015). We therefore have to rely on a discretized version of the Navier-Stokes equations with a parameterization of the unresolved subgrid scale processes. There is a wide range of subgrid scale processes and they all need to fully understood in order to build a numerical model capable of accurately simulate the ocean circulation. There are also limitations on how the ocean model interacts with other components of the climate system such as the atmosphere and sea ice.

The spatial and temporal scales that one can currently model therefore depends on the application. On global and basin scales, high horizontal resolution (usually 1/10° to 1/25°, and rarely 1/50°) is mostly used in short integrations (years to decades) with an emphasis on oceanic variability and an accurate depiction of meandering fronts and eddies. Short-term operational oceanography ocean forecasts (see Chassignet et al., 2018, for a review) more often than not use models that are forced with prescribed atmospheric fields. Seasonal to interannual forecasts, on the other hand, require longer integrations and coupling of the ocean model to an active atmosphere and sea ice in order to represent the variability resulting from large scale air-sea interactions. Coarser resolution (1/4° to 1°) is mostly used in long integrations of fully coupled ocean-sea ice-atmosphere models for climate applications (Griffies et al., 2000).

3. Global configuration

In theory, high-resolution simulations should provide results that are in better agreement with observations than low-resolution ones since truncations errors are reduced (Fox-Kemper et al., 2019). Over the past decade, access to high performance computing has made eddying resolution (i.e., ~1/10°) in ocean-sea ice models routinely possible over most of the earth, therefore allowing for a better representation of western boundary currents and associated variability. There are a few global models that have been run at higher resolution, but only for a few years, i.e. at 1/25° (Thoppil et al., 2011; Chassignet et al., 2014; Arbic et al., 2018) mostly in the context of ocean prediction, or more recently, at 1/48° (Torres et al., 2018; Qiu et al., 2018, 2020) for the study of unbalanced motions. The question then arises as to what extent the spatial resolution of the ocean model impacts climate model simulations over centennial to millennial time scales. Chassignet et al. (2020a) made a first attempt to answer this question by assessing the improvements resulting from an increase in horizontal resolution from coarse (~1º) to eddying (~0.1º) in a suite of four numerical models[1] all forced by the same atmospheric forcing dataset (JRA55-do; Tsujino et al., 2018). Parameters in the high-resolution simulations were chosen to be similar to that of their low-resolution counterparts to isolate the impact of the increase in resolution (see Chassignet et al. (2020a) for details). In the remainder of this section, we summarize the salient points of Chassignet et al. (2020a).

Overall, the broad patterns of the large scale circulation are well simulated in all experiments. When the resolution is increased, the representation of the western boundary currents (Gulf Stream and Kuroshio) is significantly improved and eddies form throughout the global domain via baroclinic instabilities since the grid spacing resolves the Rossby radius of deformation almost everywhere. A well-known feature present in many coarse resolution ocean models is an overshooting Gulf Stream and a zonal North Atlantic Current (NAC) at the Northwest Corner. This is indeed the case in three out of the four models (Figure 1) where the modeled NAC is mostly zonal and does not turn north-northeastward along the continental rise of the Grand Banks past the

[1] The four models that participated in the comparison are: the HYbrid Coordinate Ocean Model (HYCOM) (Bleck, 2002; Chassignet et al., 2003), the ocean (POP) and sea-ice components of the Community Earth System Model version 2 (CESM2; Danabasoglu et al. 2020), the ocean-sea ice component (FESOM) of the coupled Alfred Wegener Institute Climate Model (AWI-CM, Sidorenko et al., 2015, 2018; Rackow et al., 2018, 2019; Sein et al., 2018), and the LASG/IAP Climate system Ocean Model (LICOM) (Zhang and Liang,1989; Liu et al., 2004, 2012; Yu et al., 2018; Lin et al., 2020).

Flemish Cap (see Rossby (1996) for a review). This introduces a systematic heat flux bias in climate models, but one that cannot necessarily being taken care by an increase in horizontal resolution. An increase in the horizontal resolution does improve the Gulf Stream separation (see Chassignet and Marshall (2008) and Chassignet and Xu (2017) for a review) in all models, but not the North Atlantic current pathway at Northwest Corner. Only one model (HYCOM) is able to have a good representation of the Northwest Corner circulation; the North Atlantic current remains quite zonal in the other three models as the resolution is increased (Figure 1). Since the same atmospheric forcing dataset is used in all models, this seems to indicate that these differences between the models may be due to choices in model numerics, subgrid scale parameterizations, and/or sea ice representation.

As one would expect, the high-resolution experiments have much higher total kinetic energy than the low-resolution experiments (Chassignet et al., 2020a,b). In the high-resolution experiments, the range in globally averaged kinetic energy is between ~35 10^{-4} m^2/s^2 (HYCOM) and ~15 10^{-4} m^2/s^2 (LICOM). The fact that the kinetic energy is much higher in HYCOM may be due to the use of an absolute wind stress formulation in which the ocean current velocities are not taken into account. The other three models use relative winds in the wind stress formulation, which has an eddy killing effect (see Renault et al. (2020) for a review) and can reduce the total kinetic energy by as much as 30%. The total kinetic energy in these high-resolution models is however still substantially lower than what can be estimated using observations and models (~50 10^{-4} m^2/s^2) (Chassignet and Xu, 2017). The total kinetic energy increases by a factor of 3 to 4 when the resolution is increased in the models, except for the variable grid spacing FESOM which does not resolve the Rossby radius of deformation uniformly and shows an increase of a factor of 2 only.

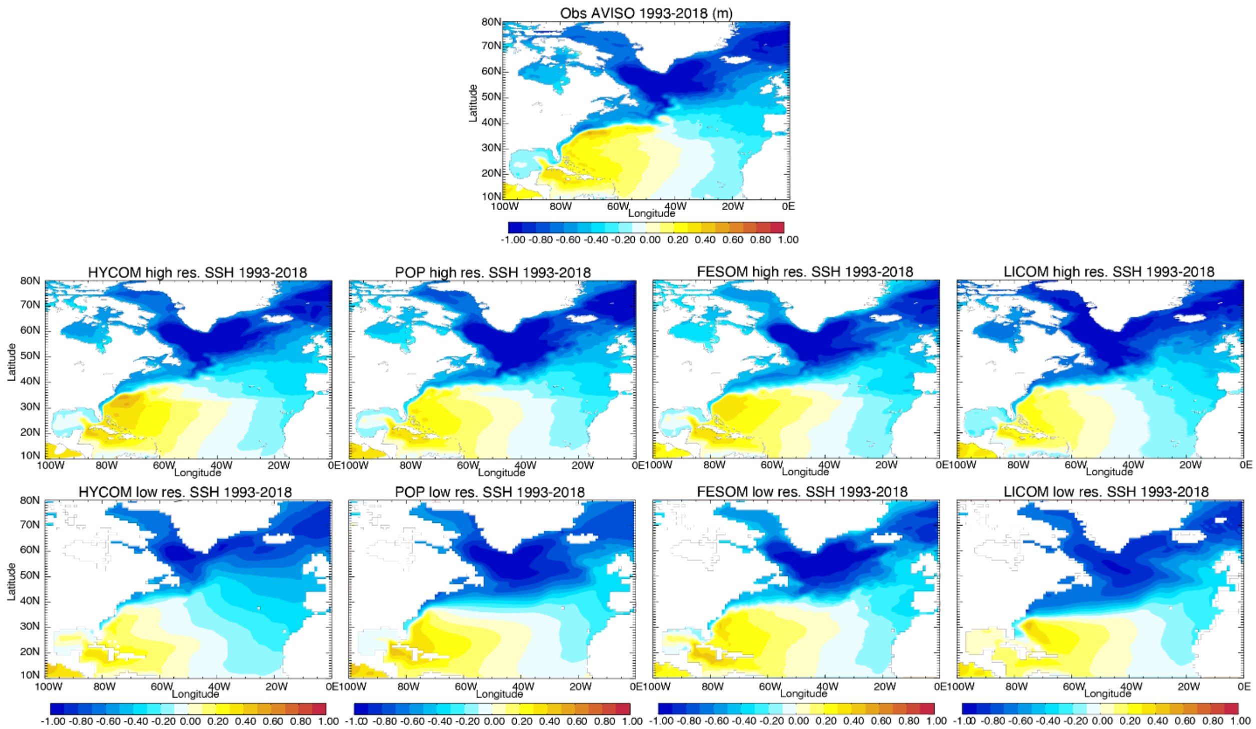

Figure 1: Mean sea surface height (SSH, in m) fields for observations (Rio et al., 2014) (top panel), high-resolution experiments (middle panel), and low-resolution experiments (lower panel). From Chassignet et al. (2020b).

Associated with the higher kinetic energy is a substantial increase in SSH variability in the high-resolution experiments. This variability is much closer to what can be observed from altimetry (Figure 2, top right panel). It is, however still lower than observed, especially in the three experiments that use relative winds (POP, FESOM, and LICOM). There are many reasons why once should take into account the vertical shear between atmospheric winds and ocean currents when computing the wind stress: first and foremost, it is more physical, but it also allows for a better representation of western boundary current systems (Ma et al., 2016). This is especially true for the Agulhas Current retroflection and associated eddies (Renault et al., 2017). When using absolute winds as in HYCOM, the Agulhas eddies shed too regularly from the Agulhas Current and follow the same pathway across the South Atlantic. This is alleviated in the three simulations with relative winds which have an Agulhas eddies pathway closer to what is observed and where the location of the Agulhas retroflection and eddy formation is more realistic.

From a climate perspective, one is especially interested in the time evolution of ocean heat content, sea level, and sea ice. The high-resolution models have a tendency to warm up more rapidly at depths below 700 m than the coarse-resolution models. Griffies et al. (2015) did find that vertical heat transport differ if the eddies are parameterized (coarse-resolution) or resolved (high-resolution) and errors in eddy subgrid scale parameterizations could therefore be responsible for this tendency. Overall, despite a significant improvement in the position, strength, and variability of western boundary currents, equatorial currents, and the Antarctic Circumpolar Current, there is no consistent improvement in temperature and salinity drift among the models when the horizontal resolution is increased. Some regions even display increased biases (see Chassignet et al. (2020a) for details). In summary, an increase in horizontal resolution does not always deliver clear bias improvement everywhere for all models.

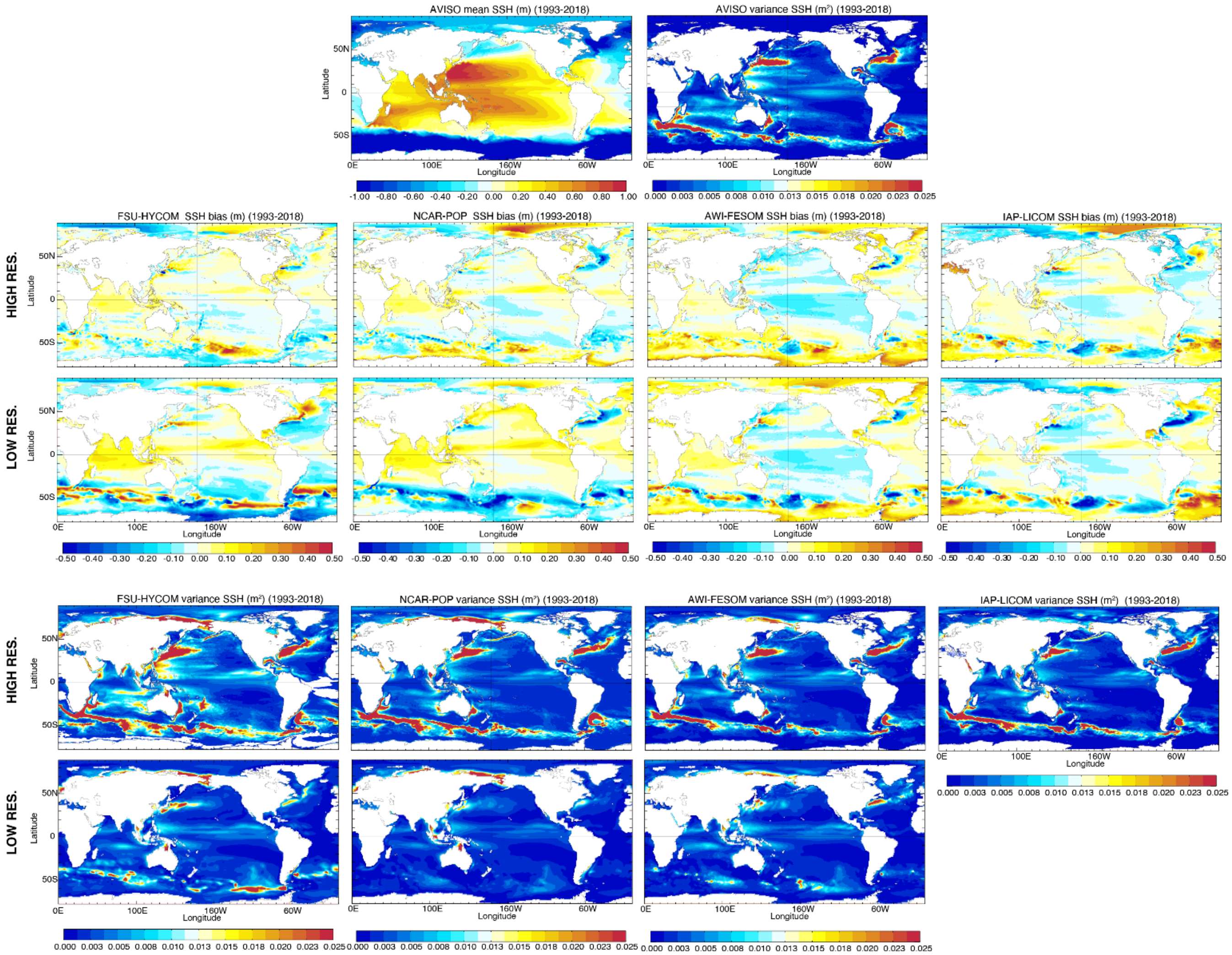

Figure 2: Top panel: Mean 1993-2018 SSH and variance AVISO. Middle panel: Difference between the mean modeled SSH and AVISO SSH. Bottom panel: Modeled variance derived from 5-day average outputs. The low-resolution LICOM SSH variance was not provided. From Chassignet et al. (2020a).

4. North and Equatorial Atlantic configuration

A smaller model domain is more computationally affordable and therefore allows more in-depth investigation of the impact of horizontal resolution (e.g., Hurlburt and Hogan, 2000; Levy et al., 2010; Chassignet and Xu, 2017; Schubert et al., 2019). Chassignet and Xu (2017), in a series of North and Equatorial Atlantic simulations, showed that, as the resolution is increased to a submesoscale-resolving 1/50° (~1.5 km at mid-latitudes) from an eddying 1/12°, the representation of the Gulf Stream penetration and associated recirculating gyres shifts from unrealistic to realistic (see legend of Figure 3 for details) and the penetration of EKE into the deep ocean is drastically improved and more closely resembles observations (see Figures 15-16 in Chassignet and Xu (2017) for details). They however noted several discrepancies between the high-resolution 1/50° numerical simulation and observations. The most notables were 1) an area of high surface EKE and/or SSH RMS wider than observed near the New England seamounts chain (Figure 4a,b) and 2) SSH surface power spectra in the 70-250 km mesoscale range independent of latitude (Figure 8). In the remainder of this section, we will show that the inclusion of high-resolution bathymetry details and tidal forcing has a strong impact on the modeled fields and significantly improve the model's ability to represent the observed ocean variability.

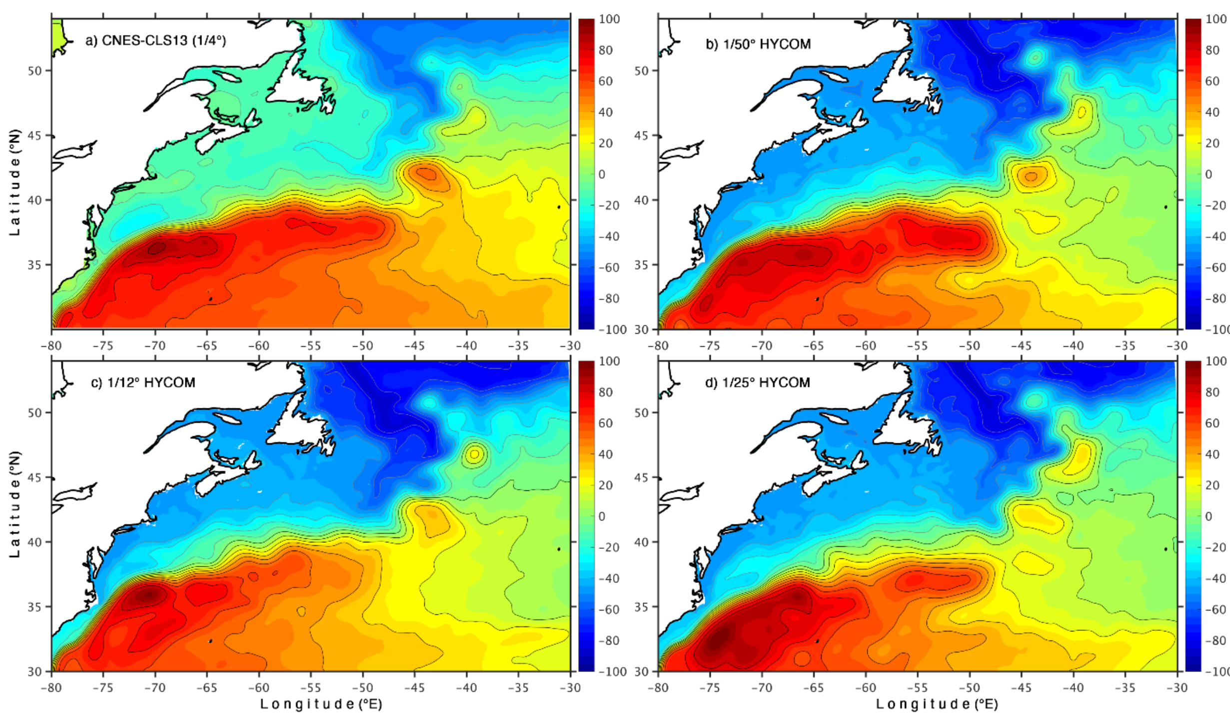

Figure 3. Mean Sea surface height (SSH, in cm) in the Gulf Stream region: (a) 1993-2012 observed mean from Rio et al. (2014), (b)1/50°, (c) 1/25°, and (d) 1/12° HYCOM (years 16-20). Adapted from Chassignet and Xu (2017). In the three simulations, the Gulf Stream separates at Cape

Hatteras, but the extent of its eastward interior penetration varies greatly. At 1/12° (Figure 3c), the modeled Gulf Stream does not extend far into the interior and the SSH variability (Figure 4c) is concentrated west of the New England seamounts (60°W). There is no visible improvement when the resolution is doubled to 1/25° (Figure 3d) simulation – on the contrary, there is an unrealistically strong recirculating gyre southeast of Cape Hatteras with excessive surface variability (Figure 4d). On the other hand, when the resolution is increased to 1/50° (Figure 3b), the Gulf Stream penetration, recirculation gyre, and extension become very realistic and compare extremely well to the latest mean dynamic topography derived from observations (Rio et al., 2014) (Figure 3a).

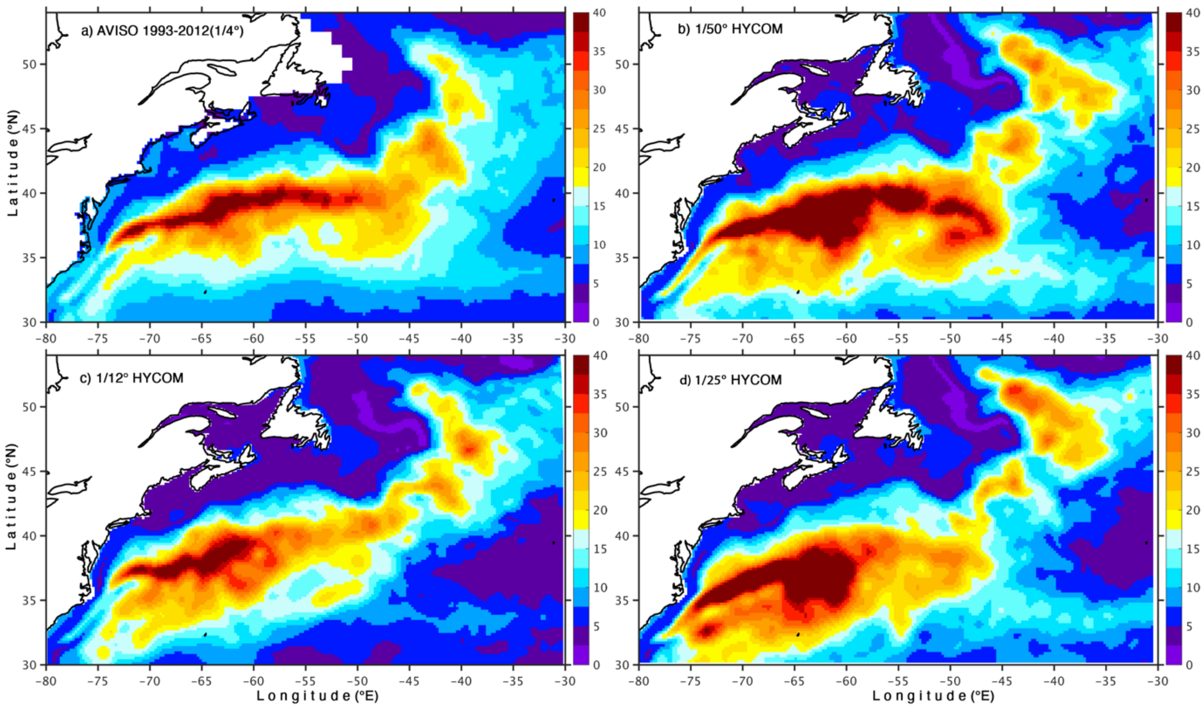

Figure 4. Sea surface height variability (in cm) in the Gulf Stream region, (a) based on AVISO (1993-2012) and (b-d) the 1/50°, 1/25°, and 1/12° HYCOM simulations, respectively (years 16-20). The model outputs were filtered to be representative of the AVISO gridded outputs by subsampling of the model outputs to the AVISO 1/4° grid, time averaging the outputs over 10 days, and applying a 150 km band pass filter.

a. *Impact of bathymetry*

The fact that the modeled high SSH variability is wider than observed near the New England seamounts chain in the 1/50° experiment (Figure 4b) suggests that interactions with the topography may be overemphasized in that specific configuration. In this section, we will show that the bathymetry has a much more profound impact on the Gulf Stream pathway than one would have a priori anticipated. In Chassignet and Xu (2017), the goal was to perform a convergence study where most parameters are not changed as the grid spacing is refined from 1/12° to 1/50° and the bathymetry used for the 1/50° configuration (hereafter referred to as NEATL) was linearly interpolated from the coarser 1/12° topography based on the 2' Naval Research Laboratory (NRL) digital bathymetry database, which combines the global topography based on satellite altimetry of Smith and Sandwell (1997) with several high-resolution regional databases. To investigate the impact of a higher-resolution bathymetry, the last 5 years of NEATL were repeated (hereafter experiment NEATL-HB) with a new bathymetry derived from the latest 15 arc-seconds GEBCO 2019 bathymetry which contains significantly higher resolution topographic features (Figure 7). All other parameters are identical to that of NEATL (see Chassignet and Xu (2017) for a detailed description).

The 5-year mean SSH for NEATL (coarse bathymetry) and NEATL-HB (fine bathymetry) are shown in Figure 5 together with the latest observational estimate (Rio et al., 2014). Overall, both agree well with the observed mean (Figure 5a), but there is a significant difference in the Gulf Stream mean pathway between the two simulations when the Gulf Stream crosses over the New England seamounts chain (area highlighted in the bottom two panels of Figure 5). The SSH contours are much closer to each other and the Gulf Stream pathway is tighter in the high-resolution bathymetry experiment NEATL-HB than in the reference experiment NEATL with coarse linearly interpolated 1/12° bathymetry. The impact of the bathymetry is further illustrated by and is more striking in the plots of SSH variability for the last 5 years of both simulations (Figure 6). Not only is the excess SSH variability near of the New England seamounts chain found in the experiment with coarse bathymetry (NEATL) gone, the shape of the variability and distribution of the variability in the experiment with high-resolution bathymetry is a very close match to the observations. This includes a deflection of the SSH variability to the north near 64°W when the Gulf Stream passes over the New England seamounts chain (see highlight in Figures 5 and 6).

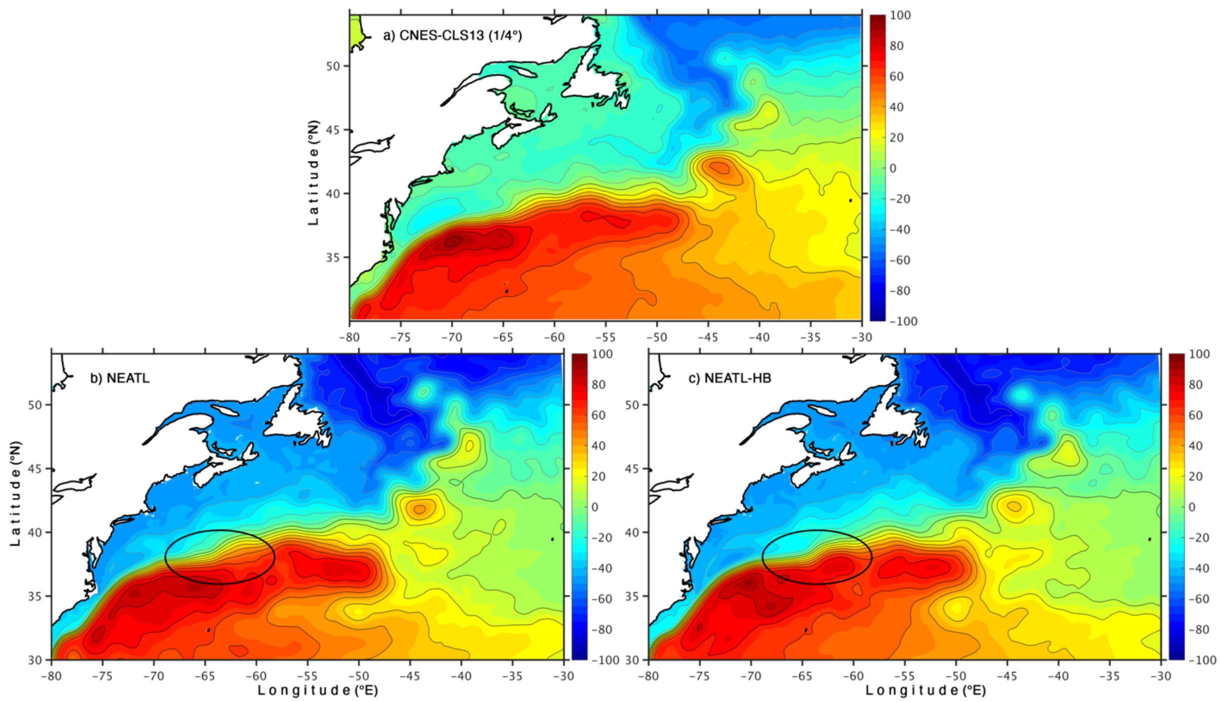

Figure 5. Mean Sea surface height (SSH, in cm) in the Gulf Stream region for (a) based on observations (1993-2012; Rio et al., 2014), (b) NEATL, and (c) NEATL-HB (years 16-20).

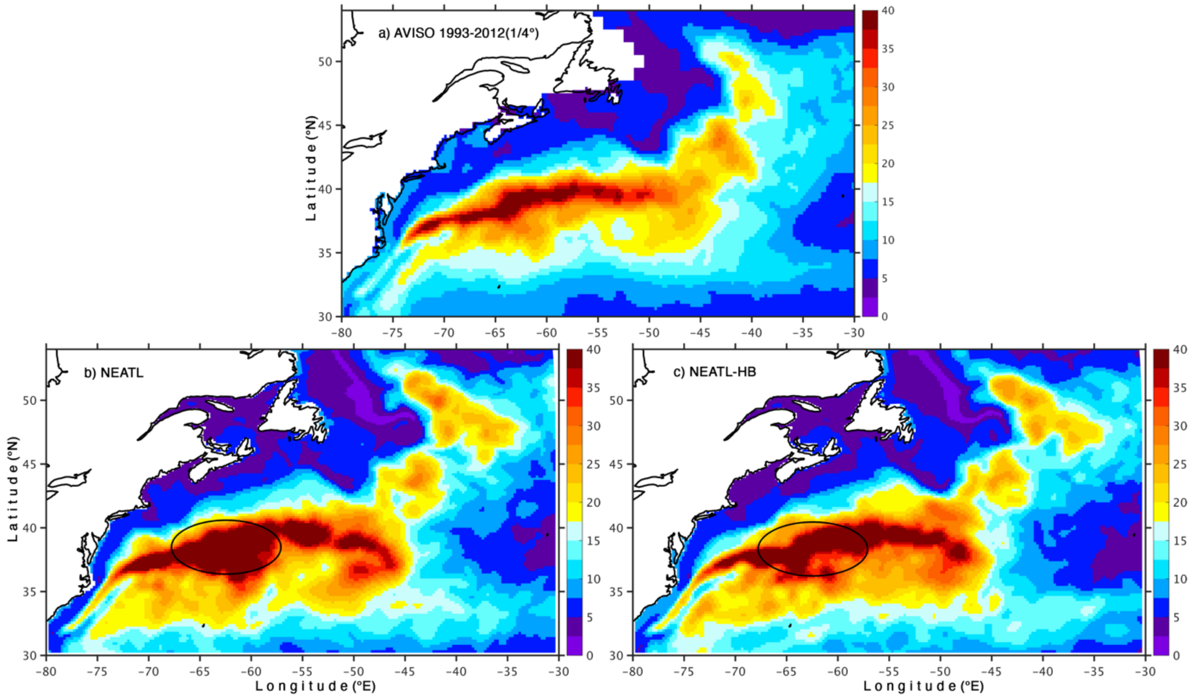

Figure 6. Sea surface height variability (SSH, in cm) in the Gulf Stream region for a) AVISO (1993-2012), b) NEATL, and c) NEATL-HB (years 16-20). The model outputs were filtered as in Figure 4.

The difference in bathymetry between the two experiments is shown in Figure 7c for the New England seamounts area. In many respects, the differences are quite small, less than a 100 m in most areas where the depth is close to 5000 m, with the biggest magnitude being around the seamounts. The bathymetry cross-section along the seamount chain (Figure 7d) shows that the most striking difference is in the height of the seamounts (500 m higher in the water column) which are closer in NEATL-HB to the base of the permanent thermocline of 1000-1500 meters (Meinen and Luther, 2016). But the higher resolution bathymetry also better resolves the spatial extent of the New England seamounts (Figure 7a,b) making them narrower and effectively increasing the separation distance between them, especially for the seamounts located between 62 and 63.5°W, i.e., Atlantis II, Shelldrake, and Gosnold (Figure 7b), that are located under the southern extent of the Gulf Stream. We interpret the difference in SSH variability between the two experiments

NEATL and NEATL-HB as follows: In the coarse bathymetry experiment NEATL, the three seamounts (Atlantis II, Shelldrake, and Gosnold) between 62 and 63.5°W are not clearly separated from each other and therefore, as discussed by Zhang and Boyer (1991), can act as a single body and will appear as a large obstacle to the eastward flowing Gulf Stream. This in turn leads to larger meanders downstream of the seamounts via conservation of potential vorticity (Holton and Hakim, 2012) and consequently higher eddy kinetic energy downstream (Barthel et al., 2017). In the high-resolution bathymetry experiment, there is a larger separation distance between the seamounts and the resulting flow field past the seamounts is determined by the interaction of the stream with relatively independent narrow obstacles and therefore less variability downstream (Zhang and Boyer, 1991). Thus, the instability processes induced by the Gulf Stream interacting with the New England seamounts are significantly diminished with better resolved topographic features and isolated seamounts. The reduced instabilities lead to a tighter Gulf Stream mean path that agrees better with the observed path and a narrower extent of high surface eddy kinetic energy that is in excellent agreement with the observations.

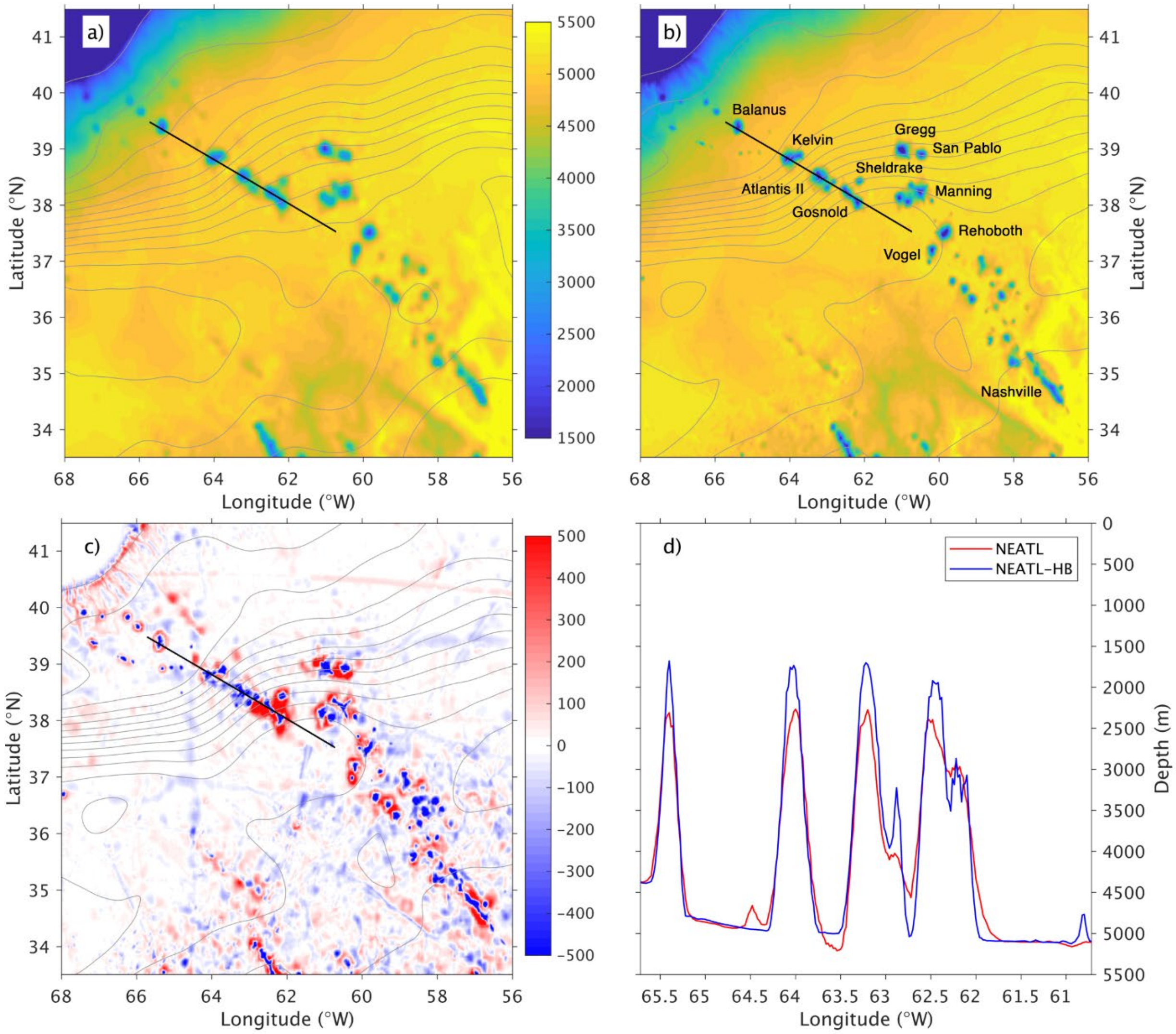

Figure 7. (a) NEATL bathymetry in meters; (b) NEATL-HB in meters with the names of the major seamounts (Houghton et al., 1977); (c) difference in bathymetry in meters between NEATL-HB and NEATL, blue color indicates a shallower depth in NEATL-HB and vice versa. The gray contours are the modeled 5-year mean SSH in NEAT-HB indicating the mean Gulf Stream pathway; and (d) bathymetry along the central portion of the New England seamount chain (black line in left panel) that encounters the Gulf Stream direcly. The four seamounts from west to east are Balanus, Kelvin, Atlantis II, and Gosnold.

b. Impact of tides on the SSH wavenumber spectra

SSH wavenumber spectra are commonly used in the literature to quantify the energy and variability associated with different temporal and spatial scales. In the reference experiment NEATL, the slope of the surface power spectra in the 70-250 km mesoscale range is mostly independent of latitude and ranges between -5 and -4 (Figure 8b), only slightly flattened near the equator and in the northern North Atlantic near 60°N. However, altimeter observations (Figure 8a) show a large spatial latitudinal variability in the distribution of the SSH wavenumber spectra with steep slopes closer to -5 at mid-latitudes and flattened slopes near -1 in the tropics (Xu and Fu, 2011, 2012; Zhou et al., 2015; Dufau et al., 2016). A lack of latitudinal dependence in the 70-250 km band with slopes between -5 and -4 was also found in previous modeling studies (Paiva et al., 1999; Richman et al., 2012, Sasaki and Klein, 2012; Biri et al., 2016) and several explanations have been put forward to explain the differences with the altimeter observations. This includes aliasing and noise in the altimetry data (Biri et al., 2016) and underestimation of the impact of high frequency motions (i.e., internal waves and tides) when using daily averages to compute the wavenumber spectra (Richman et al., 2012; Rocha et al., 2016; Tchilibou et al., 2018). Previous studies (Rocha et al., 2016; Tchilibou et al., 2018) have shown that internal tides can have a significant impact on the wavenumber spectra, especially on small scales, and we therefore further investigated the latitudinal dependence of the SSH power spectra on high-frequency motions by adding tidal forcing to the 1/50° North and Equatorial Atlantic HYCOM simulation to the last 1.5 years of NEATL (hereafter experiment (NEATL-T-HB). In NEATL-T-HB, 8 tidal constituents (M2, S2, O1, K1, N2, P1, K2, and Q1) are added via body and lateral boundary forcing. At the northern and southern boundaries, the phase and amplitude are specified using the TPXO8-atlas global tidal solutions from Oregon State University. All other parameters are identical to that of NEATL (see Chassignet and Xu (2017) for a detailed description).

Figure 8 shows the slope of the SSH wavenumber spectra in the 70-250 km mesoscale range in 10°x10° boxes over the North Atlantic domain from both NEATL and NEATL-T-HB. The latitudinal dependence is drastically different in NEATL-T-HB from that of the reference experiment with slopes that are close to -1 in the tropics as in the observations (Figure 8a). This is due to tidal forcing and the generation of internal tides since the addition of high-resolution bathymetry alone was found to have only a very small impact on the slope of SSH power spectra in the 70-250 km mesoscale range (sensitivity experiment not shown). The tidal forcing in NEATL-T-HB generate internal tides that have a strong surface SSH signature (Figure 9, bottom panel) that is not present in the absence of tidal forcing (Figure 9, top panel). These internal tides are generated in areas of strong topography around the Azores, the Cape Verde islands, off the North Brazil coast near the Amazon estuary, as well on the northern side of the Georges Bank past the New England seamounts. The surface signal associated with the internal tides modifies significantly the power spectra in the equatorial region (Figure 10) with two peaks, one in the 110-130 km range and another one in near 70 km, which flatten the slope in the equatorial region (Figure 8c). This leads to a modeled spectral slope in the equatorial region that is in excellent agreement with the filtered observational estimate of Zhou et al. (2015) (Figures 8 and 10). The impact of the internal tides on the power spectra is not as large in mid-latitudes (Figure 8) because the magnitude of the SSH variability is lower in the equatorial region than in mid-latitudes (see Figure 26 of Chassignet and Xu (2017) for details).

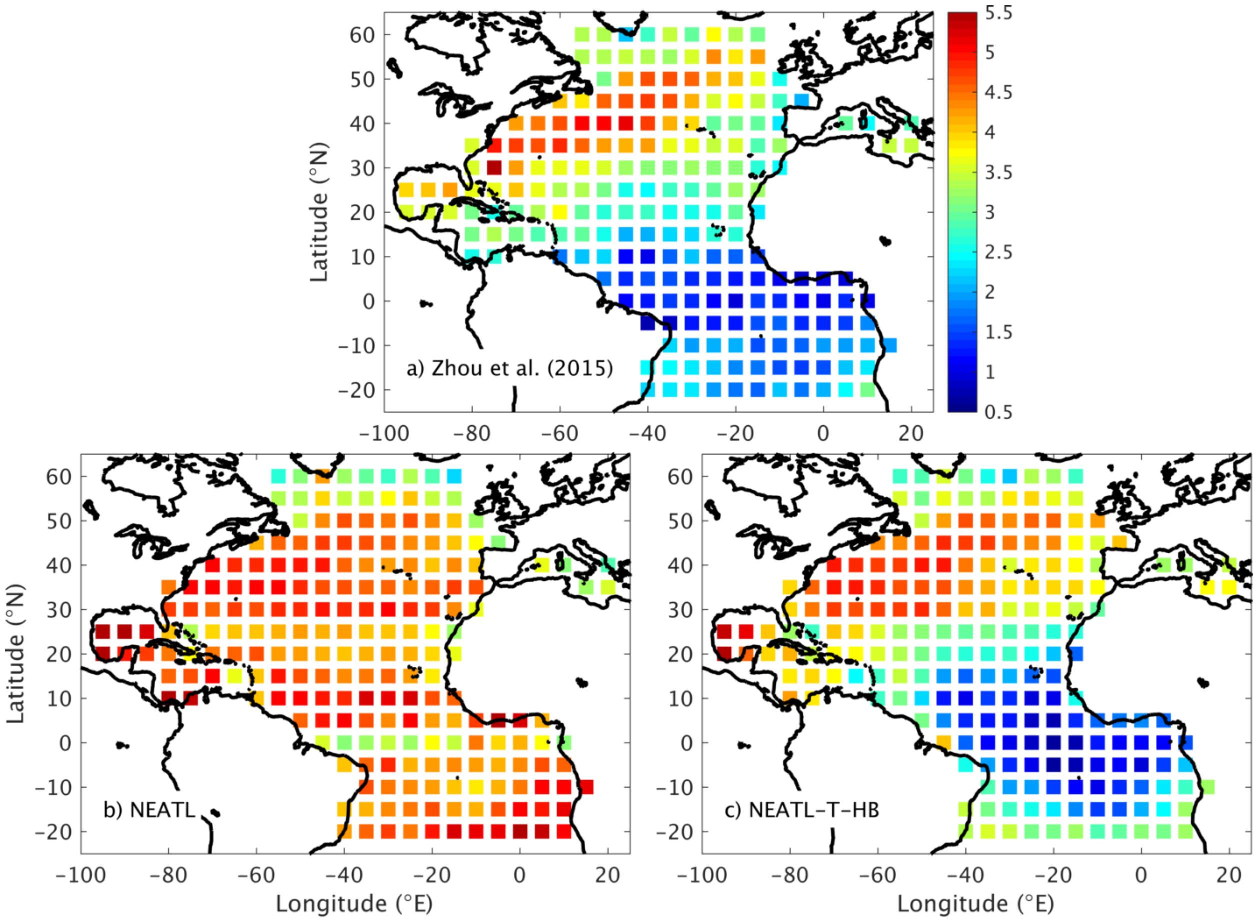

Figure 8. Slope of the sea surface height (SSH) power spectra in the 70-250 km mesoscale range in 10°x10° boxes: a) observational estimate of Zhou et al. (2015); b) NEATL, and c) NEATL-T-HB. Note that the sign of the slope was reversed.

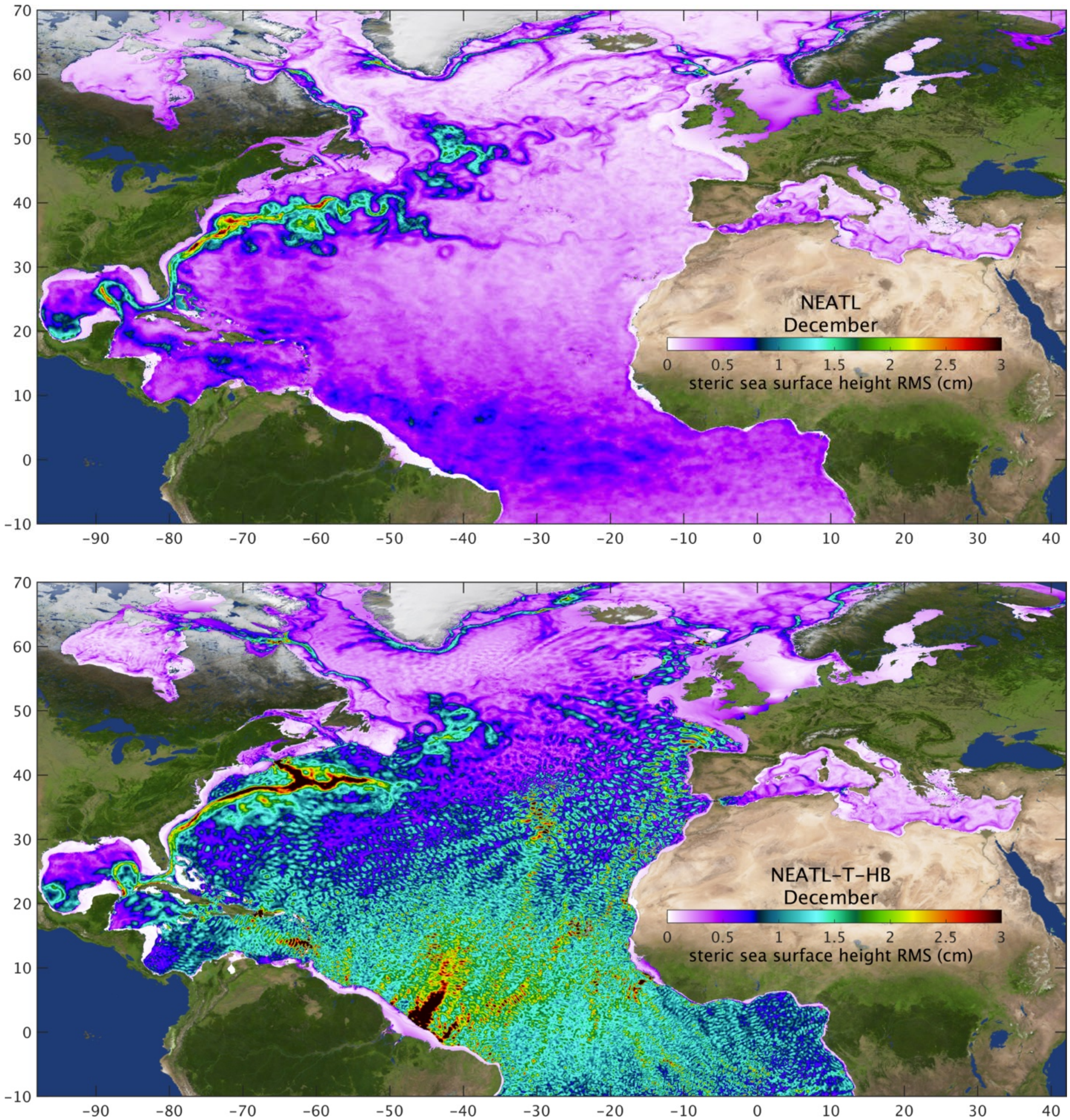

Figure 9. Root mean square (RMS) of the high-frequency steric SSH variability (in cm) for NEATL (top panel) and NEATL-T-HB (bottom panel). The RMS is calculated daily from 24 hourly snapshots of the steric SSH and is averaged over a month (December) - the results do not change if a longer time average is used.

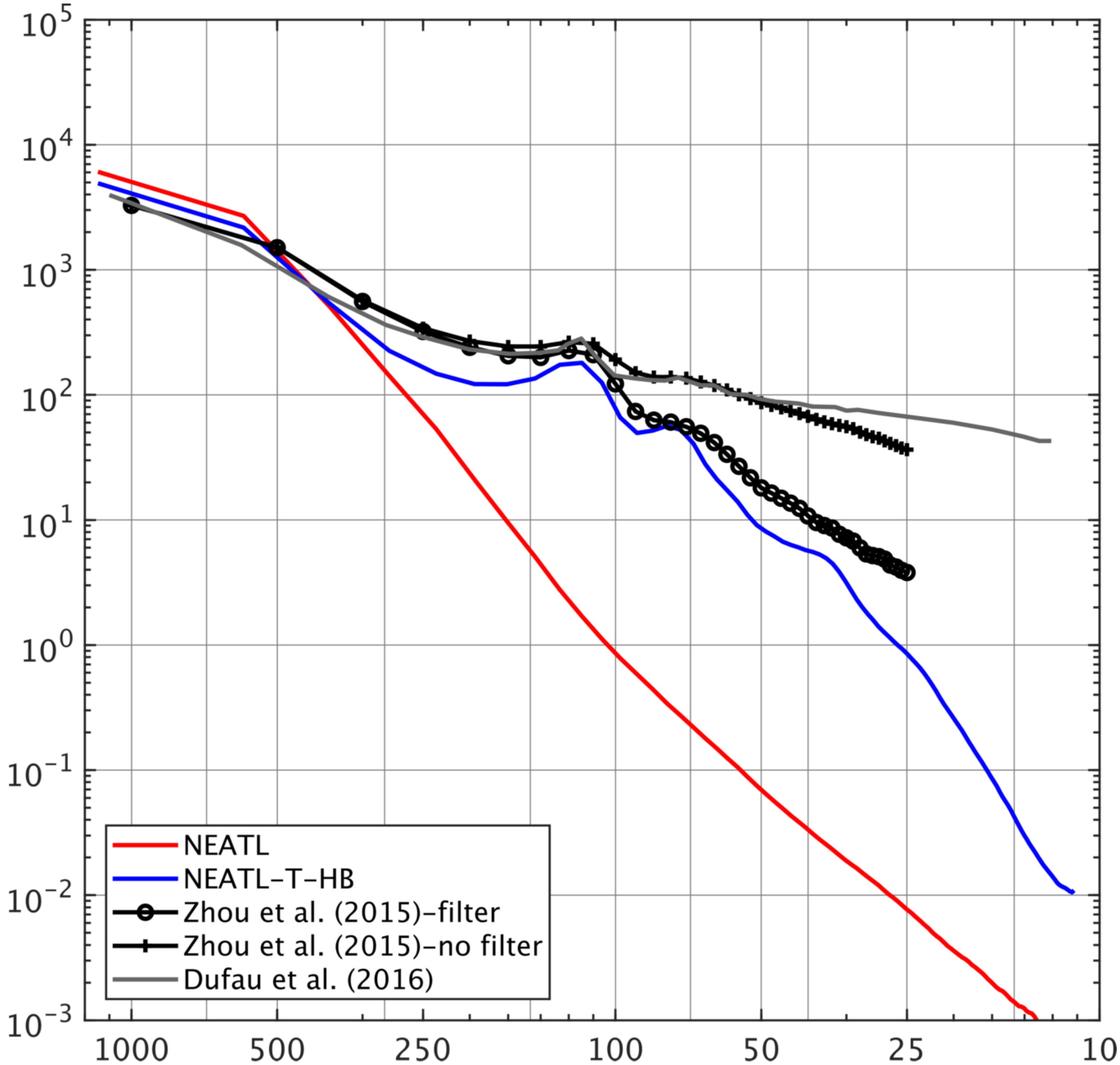

Figure 10. SSH power spectra calculated along altimeter tracks and computed as a four 10°x10° boxes average across the equator (35-15°W, 10°S-10°N). Red and blue lines are results for year 20 of NEATL and NEATL-T-HB; the black lines are observations (unfiltered and filtered for noise) by Zhou et al. (2015); and the gray line are unfiltered observations from Dufau et al. (2016).

5. Outlook

As stated in Chassignet and Xu (2017) and further supported by the additional experiments reported here, it is clear there is a substantial improvement in the models' ability to represent the observed ocean variability and western boundary currents when the horizontal resolution is increased from the eddying 1/10° to submesoscale enabled 1/50° grid spacing. As stated in Stewart et al. (2017), it is important to resolve the vertical structure of the ocean currents in accordance to the baroclinic modal decomposition that can be resolved by the horizontal grid. In other words, the finer the grid spacing, the higher the number of vertical modes one can resolve, and consequently the vertical grid spacing needs to be chosen accordingly in order to properly capture the baroclinic dynamics of a given mode. For the HYCOM experiments reported here, the vertical resolution is lower than what is recommended by Stewart et al. (2017) for z-coordinate models, but the statistics of the eddy scales and the vertical structure of the resolved eddy motions are well captured by the HYCOM layer discretization when compared to a z-coordinate kilometric model with 300 levels (Ajayi et al., 2020a,b). Furthermore, when trying to isolate the effects of horizontal resolution, one should strive to only change the horizontal resolution and associated physics.

The considerable differences in surface EKE in the global high-resolution models of Chassignet et al. (2020a) were associated with the use of relative winds versus absolute winds. Chassignet and Xu (2017) showed that the level of EKE in the 1/50° simulation was comparable to the observations when one takes into account the aliasing associated with the altimeter sampling. However, this was obtained by using absolute wind stresses at the ocean surface which do not allow any oceanic feedback to the atmosphere via ocean current/wind shear. The use of relative winds in the wind stress can lead to a significant reduction of the surface EKE (on the order of 30%; Renault et al., 2016). This implies that the next generation of numerical simulations will need to either further increase the horizontal resolution or use less dissipative numerical operators in order be able to reach a level of EKE comparable to observations when using relative winds. In addition, the bulk formula used in this class of models do not take into account any partial re-energization of the ocean by a changing atmosphere. A parameterization of this effect was recently proposed by Renault et al. (2020), but another approach, short of coupling the ocean model to an active atmosphere (HighResMIP, Haarsma et al., 2016), is to use an intermediate complexity marine atmospheric boundary layer model as in Lemarie et al. (2020) to represent the key processes associated with air/sea interactions on characteristic oceanic scales in the ocean-only numerical simulations.

The computational cost of simulations at 1/50° is extremely large, and, while currently available computer resources do not allow for decadal global simulations at that resolution, we will soon have the ability to do so in the future. Ocean/climate models are one of the biggest users of computer resources and, as resolution is further refined, they will always require the latest generation of supercomputers. This means that further progress will only take place when the numerical codes used in ocean models take full advantage of the latest computing architecture and this implies close collaborations with computer scientists. Supercomputer development is at the present time closely linked to the performance of commodity chips (i.e., GPUs) and, because of their reduced memory access, these are not well-adapted to ocean applications. The main limitation is therefore not just the computational speed of the processors, but, as stated by LeSommer et al. (2018), it also access to memory and latency in reading/writing on disk drives (see Wang et al. (2020) for an application of a GPU-based version of LICOM3).

Acknowledgements

EPC would like to thank Dr. Hailong Liu and his colleagues for their warm welcome during EPC's visit in summer 2019 to the State Key Laboratory of Numerical Modeling for Atmospheric Sciences and Geophysical Fluid Dynamics, Institute of Atmospheric Physics, Chinese Academy of Sciences, Beijing, China. Support for this visit was made possible by the Chinese Academy of Sciences (CAS) President's International Fellowship Initiative (PIFI). This overview article is heavily influenced by and reiterates many of the key points found in articles, chapters, and review papers written by the authors. Appropriate references were made, but there are many similarities in content and style to these publications throughout this article.

References

Ajayi, A.O., J. Le Sommer, E.P. Chassignet, J.-M. Molines, X. Xu, A. Albert, and E. Cosme, 2020a. Spatial and temporal variability of the North Atlantic eddy field from two kilometric-resolution ocean models. *J. Geophys. Res*., **125**, e2019JC015827, doi:10.1029/2019JC015827.

Ajayi, A.O., J. Le Sommer, E.P. Chassignet, J.-M. Molines, X. Xu, A. Albert, and W. Dewar, 2020b. Diagnosing cross-scale kinetic energy exchanges from two submesoscale permitting ocean models. *J. Adv. Model. Earth Syst*., doi:10.1002/essoar.10501077.1, revised.

Arbic, B.K., et al., 2018: A primer on global internal tide and internal gravity wave continuum modeling in HYCOM and MITgcm. In "*New Frontiers in Operational Oceanography*", E. Chassignet, A. Pascual, J. Tintoré, and J. Verron, Eds., GODAE OceanView, 307-392, doi:10.17125/gov2018.ch13.

Barthel, A., A. McC. Hogg, S. Waterman, and S. Keating, 2017: Jet–topography interactions affect energy pathways to the deep Southern Ocean. *J. Phys. Oceanogr*., **47**, 1799–1816, doi:10.1175/JPO-D-16-0220.1.

Biri, S., N. Serra, M.G. Scharffenberg, and D. Stammer, 2016: Atlantic sea surface height and velocity spectra inferred from satellite altimetry and a hierarchy of numerical simulations. *J. Geophys. Res*., **121**, 4157-4177.

Bleck, R., 2002: An oceanic general circulation model framed in hybrid isopycnic-Cartesian coordinates. *Ocean Modelling*, **37**, 55–88.

Capet, X., J.C. McWilliams, M.J. Molemaker, A.F. Shchepetkin, 2008: Mesoscale to sub-mesoscale transition in the California current system. Part I: flow structure, eddy flux, and observational tests. *J. Phys. Oceanogr.*, **38**, 29–43.

Capet, X., G. Roullet, P. Klein, and G. Maze, 2016: Intensification of upper-ocean submesoscale turbulence through Charney baroclinic instability. *J. Phys. Oceanogr.*, **46**, 33-65-3384.

Carnes, M.R., 2009: Description and evaluation of GDEM-V3.0. Naval Research Laboratory Memo. Rep. NRL/MR/7330–09-9165, 21 pp. [Available online at http://www7320.nrlssc.navy.mil/pubs/2009/carnes-2009.pdf.]

Chassignet, E. P., and Z. D. Garraffo, 2001: Viscosity parameterization and the Gulf Stream separation. In "*From Stirring to Mixing in a Stratified Ocean*", Proceedings 'Aha Huliko'a Hawaiian Winter Workshop, U. of Hawaii, January 15-19, 2001, P. Muller and D. Henderson, Eds., 37-41.

Chassignet, E.P., L.T. Smith, G.R. Halliwell, and R. Bleck, 2003: North Atlantic simulations with the hybrid coordinate ocean model (HYCOM): Impact of the vertical coordinate choice, reference pressure, and thermobaricity. *J. Phys. Oceanogr.*, **33**, 2504–2526.

Chassignet, E.P., H.E. Hurlburt, O.M. Smedstad, G.R. Halliwell, A.J. Wallcraft, E.J. Metzger, B.O. Blanton, C. Lozano, D.B. Rao, P.J. Hogan, and A. Srinivasan, 2006: Generalized vertical coordinates for eddy-resolving global and coastal ocean forecasts. *Oceanography*, **19**, 20-31.

Chassignet, E.P., and D.P. Marshall, 2008: Gulf Stream separation in numerical ocean models. In: *Ocean Modeling in an Eddying Regime*, Hecht, M., Hasumi, H. (Eds.), AGU Monograph Series, 39–62.

Chassignet, E.P., J.G. Richman, E.J. Metzger, X. Xu, P.G. Hogan, B.K. Arbic, and A.J. Wallcraft, 2014. HYCOM high-resolution eddying simulations. *CLIVAR Exchanges*, **19**(2), 22-25.

Chassignet, E.P., and X. Xu, 2017. Impact of horizontal resolution (1/12° to 1/50°) on Gulf Stream separation, penetration, and variability. *J. Phys. Oceanogr.*, **47**, 1999-2021, doi:10.1175/JPO-D-17-0031.1.

Chassignet, E.P., A. Pascual, J. Tintoré, and J. Verron (Eds.), 2018. *New Frontiers in Operational Oceanography*. GODAE OceanView, 811 pp, doi:10.17125/gov2018

Chassignet, E.P., S.G. Yeager, B. Fox-Kemper, A. Bozec, F. Castruccio, G. Danabasoglu, C. Horvat, W.M. Kim, N. Koldunov, Y. Li, P. Lin, H. Liu, D. Sein, D. Sidorenko, Q. Wang, and X. Xu, 2020a. Impact of horizontal resolution on global ocean-sea-ice model simulations based on the experimental protocols of the Ocean Model Intercomparison Project phase 2 (OMIP-2). *Geosci. Model Dev*., **13**, 4595-4637, doi:10.5194/gmd-13-4595-2020.

Chassignet, E.P., S.G. Yeager, B. Fox-Kemper, A. Bozec, F. Castruccio, G. Danabasoglu, W.M. Kim, N. Koldunov, Y. Li, P. Lin, H. Liu, D. Sein, D. Sidorenko, Q. Wang, and X. Xu, 2020b. Impact of horizontal resolution on the energetics of global ocean-sea-ice model simulations. *CLIVAR Variations/Exchanges*, **18**(1), 23-30, doi:10.5065/g8w0-fy32.

Danabasoglu, G., Lamarque, J. -F., Bachmeister, J., Bailey, D. A., DuVivier, A. K., Edwards, J., Emmons, L. K., Fasullo, J., Garcia, R., Gettelman, A., Hannay, C., Holland, M. M., Large, W. G., Lawrence, D. M., Lenaerts, J. T. M., Lindsay, K., Lipscomb, W. H., Mills, M. J., Neale, R., Oleson, K. W., Otto-Bliesner, B., Phillips, A. S., Sacks, W., Tilmes, S., van Kampenhout, L., Vertenstein, M., Bertini, A., Dennis, J., Deser, C., Fischer, C., Fox-Kember, B., Kay, J. E., Kinnison, D., Kushner, P. J., Long, M. C., Mickelson, S., Moore, J. K., Nienhouse, E., Polvani, L., Rasch, P. J., and Strand, W. G., 2020: The Community Earth System Model version 2 (CESM2), *J. Adv. Model. Earth Sys*., **12**, e2019MS001916, https://doi.org/10.1029/2019MS001916.

Dufau, C., M. Orsztynowicz, G. Dibarboure, R. Morrow, and P.-Y. Le Traon, 2016: Mesoscale resolution capability of altimetry: Present and future, *J. Geophys. Res*., **121**, doi:10.1002/2015JC010904.

Fox-Kemper, B., R. Ferrari, and R., Hallberg, 2008: Parameterization of mixed layer eddies. Part I: Theory and diagnosis. *J. Phys. Oceanogr*., **38**, 1145–1165.

Fox-Kemper, B., A. Adcroft, C.W. Böning, E.P. Chassignet, E. Curchitser, G. Danabasoglu, C. Eden, M.H. England, R. Gerdes, R.J. Greatbatch, S.M. Griffies, R. Hallberg, E. Hanert, P. Heimbach, H.T. Hewitt, C.N. Hill, Y. Komuro, S. Legg, J. Le Sommer, S. Masina, S.J. Marsland, S.G. Penny, F. Qiao, T.D. Ringler, A.M. Treguier, H. Tsujino, P. Uotila, and S.G. Yeager, 2019. Challenges and prospects in ocean circulation models. *Front. Mar. Sci*., **6:**65, doi:10.3389/fmars.2019.00065.

Griffies, S.M., C. Böning, F.O. Bryan, E.P. Chassignet, R. Gerdes, H. Hasumi, A. Hirst, A.-M. Treguier, and D. Webb, 2000. Developments in ocean climate modelling. *Ocean Modelling*, **2**, 123-192.

Griffies, S. M., Biastoch, A., Böning, C., Bryan, F., Danabasoglu, G., Chassignet, E. P., England, M. H., Gerdes, R., Haak, H., Hallberg, R. W., Hazeleger, W., Jungclaus, J., Large, W. G., Madec, G., Pirani, A., Samuels, B. L., Scheinert, M., Gupta, A. Sen, Severijns, C. A., Simmons, H. L., Treguier, A. M., Winton, M., Yeager, S. and Yin, J., 2009: Coordinated Ocean-ice Reference Experiments (COREs), *Ocean Model*., **26**(1–2), 1–46, doi:10.1016/j.ocemod.2008.08.007.

Griffies, S. M., Winton, M., Anderson, W. G., Benson, R., Delworth, T. L., Dufour, C. O., Dunne, J. P., Goddard, P., Morrison, A. K., Rosati, A., Wittenberg, A. T., Yin, J. J. and Zhang, R., 2015: Impacts on ocean heat from transient mesoscale eddies in a hierarchy of climate models, *J. Clim*., **28**, 952-977.

Haarsma, R. J., Roberts, M. J., Vidale, P. L., Senior, C. A., Bellucci, A., Bao, Q., Chang, P., Corti, S., Fučkar, N. S., Guemas, V., von Hardenberg, J., Hazeleger, W., Kodama, C., Koenigk, T., Leung, L. R., Lu, J., Luo, J.-J., Mao, J., Mizielinski, M. S., Mizuta, R., Nobre, P., Satoh, M., Scoccimarro, E., Semmler, T., Small, J. and von Storch, J.-S., 2016: High Resolution Model Intercomparison Project (HighResMIP v1.0) for CMIP6, Geosci. Model Dev., 9(11), 4185–4208, doi:10.5194/gmd-9-4185-2016.

Hallberg, R., 2013: Using a resolution function to regulate parameterizations of oceanic mesoscale eddy effects. *Ocean Modelling*, **72**, doi:10.1016/j.ocemod.2013.08.007.

Holton, J.R., and G.J. Hakim, 2012: *An introduction to dynamic meteorology*, Elsevier Science, 552pp, ISBN-13:9780123848666.

Houghton, R. L., Thompson, G., and Bryan, W. B., 1977. Petrological and geochemical studies of the New England Seamount Chain, *AGU Trans*, **58**, 530.

Hurlburt, H. E., and P. J. Hogan, 2000: Impact of 1/8° to 1/64° resolution on Gulf Stream model-data comparisons in basin-scale subtropical Atlantic ocean models. *Dyn. Atmos. Oceans*, **32**, 283-329.

Kara, A.B., Wallcraft, A.J. and Hurlburt, H.E. 2005: A new solar radiation penetration scheme for use in ocean mixed layer studies: an application to the Black Sea using a fine resolution Hybrid Coordinate Ocean Model (HYCOM). *J. Phys. Oceanogr*., **35**, 13–32.

Klein, P., G. Lapeyre, G. Roullet, S. Le Gentil, and H. Sasaki, 2011: Ocean turbulence at meso and submesoscales: Connection between surface and interior dynamics, *Geophys. Astrophys. Fluid Dyn*., **105**, 421–437.

Large, W.G., J.C. McWilliams, and S.C. Doney, 1994: Ocean vertical mixing: a review and a model with a nonlocal boundary layer parameterization. *Rev. Geophys*., **32**, 363–403.

Lemarié, F., Samson, G., Redelsperger, J.-L., Giordani, H., Brivoal, T., and Madec, G., 2020: A simplified atmospheric boundary layer model for an improved representation of air-sea interactions in eddying oceanic models: implementation and first evaluation in NEMO (4.0), *Geosci. Model Dev. Discuss*., https://doi.org/10.5194/gmd-2020-210, in review.

Le Sommer, J., E.P. Chassignet, and A.J. Wallcraft, 2018. Ocean circulation modeling for operational oceanography: Current status and future challenges. In "*New Frontiers in Operational Oceanography*", E. Chassignet, A. Pascual, J. Tintoré, and J. Verron (Eds.), GODAE OceanView, 289-306, doi:10.17125/gov2018.ch12.

Lévy M., P. Klein, A.-M. Tréguier, D. Iovino, G. Madec, S. Masson, and K. Takahashi, 2010: Modifications of gyre circulation by sub-mesoscale physics. *Ocean Modelling*, **34**, 1-15.

Lin, P. F., Yu, Z., Liu, H., Yu, Y., Li, Y,Jiang, J., Xue, W., Chen, K., Yang, Q., Zhao, B., Wei, J., Ding, M., Sun, Z., Wang, Y., Meng, Y., Zheng, W., and Ma, J, 2020: LICOM model datasets for the CMIP6 Ocean model intercomparison project, Adv. Atmos. Sci., 37, 239-−249, https://doi.org/10.1007/s00376-019-9208-5.

Liu, H. L., Zhang, X. H., Li, W., Yu, Y. Q., and Yu, R. C., 2004: An eddy-permitting oceanic general circulation model and its preliminary evaluation, Adv. Atmos. Sci., 21, 675–690, https://doi.org/10.1007/bf02916365.

Liu, H., Lin, P., Yu, Y., and Zhang, X., 2012: The baseline evaluation of LASG/IAP Climate system Ocean Model (LICOM) version 2, Acta Meteorol. Sin., 26, 318–329, https://doi.org/10.1007/s13351-012-0305-y.

Ma, X., Z. Jing, P. Chang, X. Liu, R. Montuoro, R.J. Small,F.O. Bryan, R.J. Greatbatch, P. Brandt, D. Wu, X. Lin, and L. Wu, 2016: Western boundary currents regulated by interaction between ocean eddies and the atmosphere. *Nature*, **535**, 533–537. doi:10.1038/nature18640.

Meinen, C. S., and Luther, D. S., 2016. Structure, transport and vertical coherence of the Gulf Stream from the Straits of Florida to the Southeast Newfoundland Ridge. *Deep-Sea Research* Part I, **111**, 16– 33, doi:10.1016/j.dsr.2016.02.002.

Paiva, A.M., J.T. Hargrove, E.P. Chassignet, and R. Bleck, 1999: Turbulent behavior of a fine mesh (1/12°) numerical simulation of the North Atlantic. *J. Mar. Sys*., **21**, 307–320.

Qiu, B., S. Chen, P. Klein, J. Wang, H. Torres, L.-L. Fu and D. Menemenlis, 2018: Seasonality in transition scale from balanced to unbalanced motions in the world ocean. *J. Phys. Oceanogr*., **48**, 591-605.

Qiu, B., S. Chen, P. Klein, H. Torres, J. Wang, L.-L. Fu, & D. Menemenlis, 2020: Reconstructing upper ocean vertical velocity field from sea surface height in the presence of unbalanced motion. *J. Phys. Oceanogr*., **50**, 55-79.

Rackow, T., Goessling, H. F., Jung, T., Sidorenko, D., Semmler, T., Barbi, D., and Handorf, D., 2018: Towards multi-resolution global climate modeling with ECHAM6-FESOM. Part II: climate variability, *Clim. Dyn*., **50**, 2369–2394, https://doi.org/10.1007/s00382- 016-3192-6.

Rackow, T., Sein, D. V., Semmler, T., Danilov, S., Koldunov, N. V., Sidorenko, D., Wang, Q., and Jung, T., 2019: Sensitivity of deep ocean biases to horizontal resolution in prototype CMIP6 simulations with AWI-CM1.0, *Geosci. Model Dev*., **12**, 2635–2656, https://doi.org/10.5194/gmd-12-2635-2019.

Renault, L., McWilliams, J. C. and Penven, P., 2017: Modulation of the Agulhas Current retroflection and leakage by oceanic current interaction with the atmosphere in coupled simulations, *J. Phys. Oceanogr*., **47**(8), 2077–2100, doi:10.1175/JPO-D-16-0168.1.

Renault, L., Masson, S., Arsouze, T., Madec, G., and McWilliams, J. C., 2020: Recipes for how to force oceanic model dynamics, *J. Adv. Model. Earth Sy*., 2019MS001715, doi:10.1029/2019MS001715.

Richman, J.G., B.K. Arbic, J.F. Shriver, E.J. Metzger, and A.J. Wallcraft, 2012: Inferring dynamics from the wavenumber spectra of an eddying global ocean model with embedded tides. *J. Geophys. Res*., **117**, C12012, doi:10.1029/2012JC008364.

Rio, M.-H., S. Mulet, and N. Picot, 2014: Beyond GOCE for the ocean circulation estimate: Synergetic use of altimetry, gravimetry, and in situ data provides new insight into geostrophic and Ekman currents. *Geophys. Res. Lett*., **41**, 8918–8925, doi:10.1002/2014GL061773.

Rocha, C.B., T.K. Chereskin, S.T. Gille, and D. Menemenlis, 2016: Mesoscale to submesoscale wavenumber spectra in Drake Passage, *J. Phys. Oceanogr*., **46**, 601-620.

Rossby, T., 1996: The North Atlantic Current and surrounding waters: At the crossroads, Rev. Geophys., 34, 463–481, https://doi.org/10.1029/96RG02214.

Roullet, G., J.C. McWilliams, X. Capet and M.J. Molemaker, 2012: Properties of equilibrium geostrophic turbulence with isopycnal outcropping. *J. Phys. Oceanogr.*, **42**, 18-38, 2012.

Sasaki, H., and P. Klein, 2012: SSH wavenumber Spectra in the North Pacific from a high-resolution realistic simulation, *J. Phys. Oceanogr.*, **42** (7): 1233-1241, https://doi.org/10.1175/JPO-D-11-0180.1

Schubert, R., Schwarzkopf, F. U., Baschek, B., and Biastoch, A., 2019: Submesoscale Impacts on Mesoscale Agulhas Dynamics, *J. Adv. Model. Earth Syst.*, 11, 2745– 2767. doi:https://doi.org/10.1029/2019MS001724.

Sein, D. V., Koldunov, N. V., Danilov, S., Sidorenko, D., Wekerle, C., Cabos, W., Rackow, T., Scholz, P., Semmler, T., Wang, Q., and Jung, T., 2018: The relative influence of atmospheric and oceanic model resolution on the circulation of the North Atlantic Ocean in a coupled climate model, *J. Adv. Model. Earth Syst.*, **10**, 2026–2041, https://doi.org/10.1029/2018MS001327.

Sidorenko, D., Rackow, T., Jung, T., Semmler, T., Barbi, D., Danilov, S., Dethloff, K., Dorn, W., Fieg, K., Goessling, H. F., Handorf, D., Harig, S., Hiller, W., Juricke, S., Losch, M., Schröter, J., Sein, D. V., and Wang, Q., 2015: Towards multi-resolution global climate modeling with ECHAM6–FESOM. Part I: model formulation and mean climate, Clim. Dynam., 44, 757–780, https://doi.org/10.1007/s00382-014-2290-6.

Sidorenko, D., Koldunov, N. V., Wang, Q., Danilov, S., Goessling, H. F., Gurses, O., Scholz, P., Sein, D. V., Volodin, E., Wekerle, C., and Jung, T., 2018: Influence of a salt plume parameterization in a coupled climate model, J. Adv. Model. Earth Sy., 10, 2357–2373, https://doi.org/10.1029/2018MS001291.

Smith, R.D., M.E. Maltrud, F.O. Bryan, and M.W. Hecht, 2000: Numerical simulation of the North Atlantic Ocean at 1/10°. *J. Phys. Oceanogr.*, **30**, 1532–1561.

Smith, W.H.F., and D.T. Sandwell, 1997: Global sea floor topography from satellite altimetry and ship depth soundings. *Science,* **277**, 1956–1962.

Smyth, W.D., J.N. Moum, and D.R. Caldwell, 2001: The efficiency of mixing in turbulent patches: Inferences from direct simulations and microstructure observations, *J. Phys. Oceanogr.*, **31**, 1969– 1992, doi:10.1175/1520-0485(2001)0312.0.CO;2.

Stewart, K. D., Hogg, A. McC., Griffies, S. M., Heerdegen, A. P., Ward, M. L., Spence, P., and England, M. H., 2017: Vertical resolution of baroclinic modes in global ocean models, *Ocean Model*., **113**, 50–65, https://doi.org/10.1016/j.ocemod.2017.03.012.

Tchilibou, M., Gourdeau, L., Morrow, R., Serazin, G., Djath, B., and Lyard, F., 2018: Spectral signatures of the tropical Pacific dynamics from model and altimetry: a focus on the meso-/submesoscale range, Ocean Sci., 14, 1283–1301, https://doi.org/10.5194/os-14-1283-2018.

Teague, W.J., M.J. Carron, and P.J. Hogan, 1990: A comparison between the generalized digital environmental model and Levitus climatologies. *J. Geophys. Res*., **95**, 148-227, doi: 10.1029/89JC03682.

Thomas, L.N., A. Tandon, and A. Mahadevan, 2008: Sub-mesoscale processes and dynamics. *Ocean Modeling in an Eddying Regime*, Hecht, M., Hasumi, H. (Eds.), AGU Monograph Series, 17-38.

Thoppil, P.G., J.G. Richman and P.J. Hogan, 2011: Energetics of a global ocean circulation model compared to observations. *Geophys. Res. Lett*., **38**, L15607, doi:10.1029/2011GL048347.

Torres, H.S., P. Klein, D. Menemenlis, B. Qiu, Z. Su, J. Wang, S. Chen, and L.-L. Fu, 2018: Partitioning ocean motions into balanced motions and internal gravity waves: A modeling study in anticipation of future space missions. *J. Geophys. Res*., **123**, http://doi.org/10.1029/2018JC014438.

Tsujino H., S. Urakawa, S.M. Griffies, G. Danabasoglu, A.J. Adcroft, A.E. Amaral, T. Arsouze, M. Bentsen, R. Bernardello, C. Böning, A. Bozec, E.P. Chassignet, S. Danilov, R. Dussib, E. Exarchou, P.G. Fogli, B. Fox-Kemper, C. Guo, M. Illicak, D. Iovino, W.M. Kim, N. Koldunov, V. Lapin, Y. Li, P. Lin, K. Lindsay, H. Liu, M.C. Long, Y. Komuro, S.J. Marsland, S. Masina, A. Nummelin, J.K. Rieck, Y. Ruprich-Robert, M. Scheinert, V. Sicardi, D. Sidorenko, T. Susuki, H. Tatebe, Q. Wang, S.G. Yeager, and Z. Yu, 2020. Evaluation of global ocean-sea-ice model simulations based on the experimental protocols of the Ocean Model Intercomparison Project phase 2 (OMIP-2). *Geosci. Model Dev*., **13**, 3643-3708, doi:10.5194/gmd-13-3643-2020.

Uppala, S.M., and Coauthors, 2005: The ERA-40 Re-Analysis. *Quart. J. Roy. Meteor. Soc*., **131**, 2961–3012, doi:10.1256/qj.04.176.

Wang, P., J. Jiang, P. Lin, M. Ding, J. Wei, F. Zhang, L. Zhao, Y. Li, Z. Yu, W. Zheng, Y. Yu, X. Chu, and H. Liu, 2020: The GPU version of LICOM3 under HIP framework and its large-scale application. *Geosci. Model Dev*., submitted.

Xu, X., W. J. Schmitz Jr., H.E. Hurlburt, P.J. Hogan, and E.P. Chassignet, 2010: Transport of Nordic Seas overflow water into and within the Irminger Sea: An eddy-resolving simulation and observations. *J. Geophys. Res*., **115**, C12048, doi:10.1029/2010JC006351.

Xu, Y., and L.-L. Fu, 2011: Global variability of the wavenumber spectrum of oceanic mesoscale turbulence. *J. Phys. Oceanogr*., **41**, 802-809, doi:10.1175/2010JPO4558.1.

Xu, Y., and L.-L. Fu, 2012: The effects of altimeter instrument noise on the estimation of the wavenumber spectrum of sea surface height, *J. Phys. Oceanogr*., **42**, 2229–2233, doi:10.1175/JPO-D-12-0106.1.

Yeung, P.K., Zhai, X.M., and Sreenivasan, K.R., 2015: Extreme events in computational turbulence. *Proc. Nat. Acad. Sci. USA*, **112**(41), 12633–12638, doi:10.1073/pnas.1517368112.

Yu, Y. Q., Tang, S. L. , Liu, H. L., Lin, P. F., and Li, X. L., 2018: Development and evaluation of the dynamic framework of an ocean general circulation model with arbitrary orthogonal curvilinear coordinate, *Chinese J. Atmos. Sci*., **42**, 877−- 889, https://doi.org/10.3878/j.issn.1006-9895.1805.17284, (in Chinese with English abstract).

Zhang, X. H. and Liang, X. Z., 1989: A numerical world ocean general circulation model, *Adv. Atmos. Sci*., **6**, 44−-61, https://doi.org/10.1007/BF02656917.

Zhang, X., and D. L. Boyer, 1991: Current deflections in the vicinity of multiple seamounts. *J. Phys. Oceanogr.*, **21**, 1122–1138, doi:10.1175/1520-0485(1991)021<1122:CDITVO>2.0.CO;2.

Zhou, X.-H., D.-P. Wang, and D. Chen, 2015: Global wavenumber spectrum with corrections for altimeter high-frequency noise. *J. Phys. Oceanogr*., **45**, 495-503.